# Supporting Information

**Small Universal Mechanical Module Driven by a Liquid Metal Droplet**

Rui Xue[a], Ye Tao[b,*], Haoxiu Sun[c], Weiyu Liu[d], Zhenyou Ge[a], Tianyi Jiang[e], Hongyuan Jiang[e], Fang Han[c], Yu Li[c,*], Yukun Ren[a,*]

[a]State Key Laboratory of Robotics and System, Harbin Institute of Technology, West Da-zhi Street 92, Harbin, Heilongjiang 150001, People's Republic of China. Email: rykhit@hit.edu.cn

[b]School of Engineering and Applied Sciences and Department of Physics Harvard University, 9 Oxford Street, Cambridge, MA 02138, USA. Email: ytao@seas.harvard.edu

[c]School of Life Sciences, Harbin Institute of Technology, No. 2 Yikuang Street, Harbin 150001, People's Republic of China. Email: liyugene@hit.edu.cn

[d] School of Electronics and Control Engineering, Chang'an University, Middle-Section of Nan'er Huan Road, Xi'an 710000Xi'an 710064, People's Republic of China.

[e]School of Mechatronics Engineering, Harbin Institute of Technology, West Da-zhi Street 92, Harbin 150001, People's Republic of China.

Keywords: Small modules, Liquid metal, Electrocappillary stress, Induced-charge electrokinetic phenomena, Cell culture

**This material gives supporting information in the paper:**

SI Appendix 1. Design and fabrication information of the driven module.

SI Appendix 2. CEW of Al-EGaIn in alkaline solution.

SI Appendix 3. Comparison of flow rate induced by the CEW of EGaIn and Al-EGaIn droplet.

SI Appendix 4. Force analysis of the power wheel.

SI Appendix 5. Real photo of the comparison channel.

SI Appendix 6. Utilizing rotational motion to drive gear.

SI Appendix 7. Real photo of the circulating channel.

SI Appendix 8. Redesign of the driven module to improve productivity.

SI Appendix 9. Biological driven module and cell culture channel.

**Supplementary movie:**

Movie S1. Operating state of the power module.

Movie S2. Comparison of pumping effect (EGaIn:Al-EGaIn).

Movie S3. The position of aluminum flake in LMD.

Movie S4. The position of LMD in the operating state.

Movie S5. Driven module in gear drive.

Movie S6. Pumping by a propeller.

Movie S7. Operating state of bio experiment.

Movie S8. Circulating pumping in the cultivation channel.

## SI Appendix 1. Design and fabrication information of the driven module

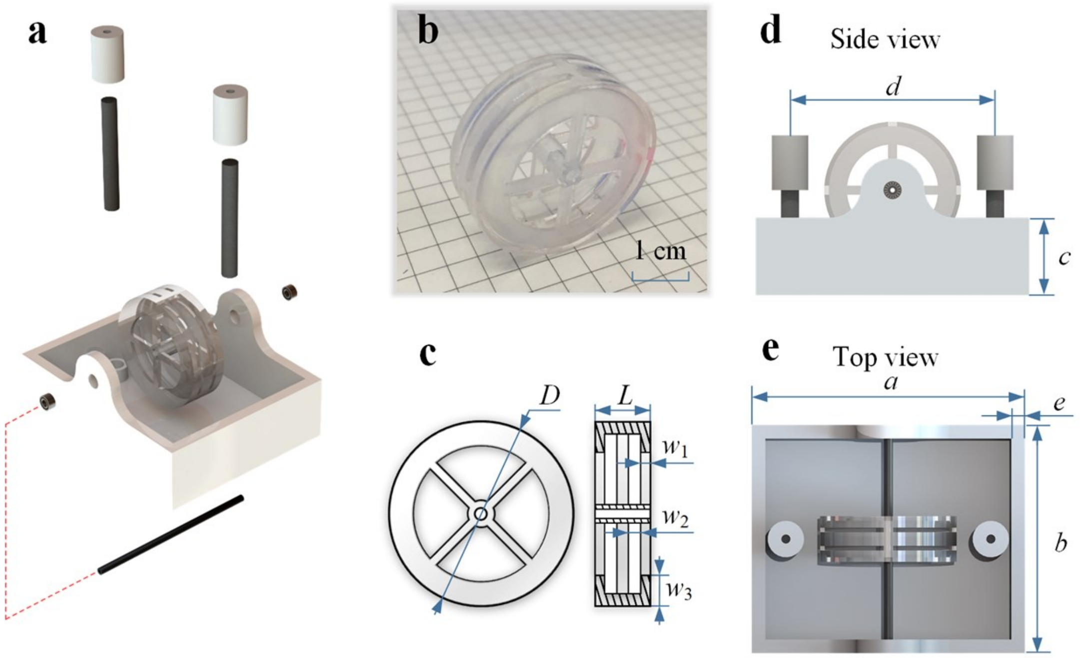


**Fig. S1.** Detailed sizes and description of each part. a) Exploded view of the power module. b) Photo of the actual wheel. c) Main view and side view of the wheel with related design size. d) Side view of the reservoir with related design size. e) Top view of the reservoir with related design size.

The power wheel is the core part of the whole driving module (Fig. S1 a) as shown in Fig. S1 b and its design parameters are displayed in Fig. S1 c and Table S1. The inner ring of the wheel is processed with a groove to hold the LMD. A pair of gaps are designed to enable the working fluid to pass through freely and forming a current path. Besides this, the gaps also increase the flow rate and reduce the viscous resistance between the droplet and wheel.

**Table S1.** Detailed sizes of the power wheel

| Parameter | D | L | $w_1$ | $w_2$ | $w_3$ |
| --- | --- | --- | --- | --- | --- |
| Size (mm) | 30 | 10 | 2 | 2 | 5 |

A side view Fig. S1 d and a top view Fig. S1 e are displayed to introduce detailed design parameters as shown in Table S2, with related fabrication information given by Table S3.

**Table S2.** the detailed size of each part

| Parameter | a | b | c | d | e |
| --- | --- | --- | --- | --- | --- |
| Origin | 65 | 30 | 30 | 50 | 2 |
| Serial arrangment | 65 | 45 | 30 | 50 | 2 |
| Parallel arrangment | 105 | 30 | 30 | 90 | 2 |
| Cell culture | 120 | 80 | 45 | 55 | 2 |

**Table S3.** Detailed material properties of each part

| Parts | Material | Distortion temperature |
| --- | --- | --- |
| Power Wheel | Photosensitive resin | 45℃ |
| Tank | Resin | 46℃ |
| Tank (bio experiment) | Nylon (waterproofing work) | 150℃ |
| Rotation Axis | Carbon fiber | 160℃ |
| Pumping wheel | Nylon | 150℃ |

## SI Appendix 2. CEW of Al-EGaIn in alkaline solution

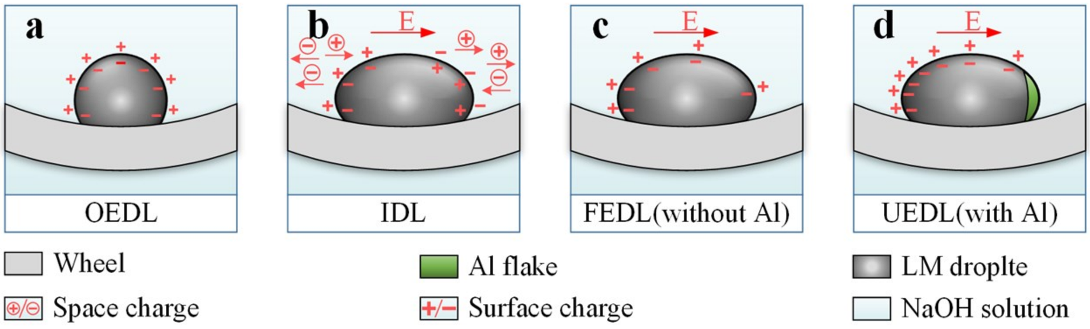


**Fig. S2.** The charge distribution on the surface of the ideally polarizable LM droplet in different stages. a) A uniformly distributed charge within OEDL. b) Formation progress of the bipolar IDL due to electrochemical polarization on the ideally polarizable surface of the LMD under DC force. c) FEDL with a nonuniform charge distribution gradient, as ascribed to a combined effect of OEDL and IDL. d) the final charge distribution of Al-EGaIn in alkaline solution under a DC signal.

Ga in the EGaIn will react with the NaOH after the oxidation film of the droplet is consumed completely in alkaline solution: $Ga + OH^- = [Ga(OH)_4]^-$ The generation of $[Ga(OH)_4]^-$ will make the conducting surface of the droplet negatively charged and attract the positive counterions from the surrounding solution to form an original electric double layer (OEDL) as shown in Fig. S2 a with a voltage drop (external-internal):

$$V_{\mathrm{OEDL}} = -\frac{q_0}{C_0} \tag{S1}$$

When the DC electric field is applied, ionic charge carriers ($OH^-$, $H^+$, and $Na^+$, mainly) will experience an oriented electrophoretic motion along or against the applied electric field lines. As the charged ions approached the LM droplet, since they are not allowed to penetrate across the phase boundary, an equal amount of polarized mirror charge has to be induced on the droplet's surface. This results in the formation of a bipolar diffuse screening cloud containing a symmetric charge of opposite sign which is called IDL as shown in Fig. S2 b. In the approximation of thin double-layer limit and small induced zeta potential, complete capacitive charging of the diffuse layer takes place, so the equal body potential $\varphi_0$ of the LMD and the voltage $\varphi$ in the fluid bulk right outside the IDL are described separately in Eq. (S2) and (S3):

$$\varphi_0 = \int_{\partial\mathrm{drop}} \varphi dS \Big/ \int_{\partial\mathrm{drop}} dS \tag{S2}$$

$$\sigma \boldsymbol{n} \cdot \nabla \varphi = 0 \tag{S3}$$

the linear superimposition of OEDL and IDL is termed the FEDL, wherein the net charge concentration gradually decreases in the direction of the electric field, corresponding to a composite double-layer voltage drop (external-internal):

$$\Delta V_{\mathrm{FEDL}} = V_{\mathrm{OEDL}} + V_{\mathrm{IEDL}} = -q_0/C_0 + (\varphi - \varphi_0) \tag{S4}$$

The charge distribution of FEDL under a unidirectional electric field is displayed in Fig. S2 c. The introduction of aluminum flakes will magnify this difference of charge distribution since aluminum can consume more negative ions like $OH^-$ at the droplet's end near the cathode resulting in many more cations to gather here. Fig. S2 d shows the final charge distribution on the Al-GaIn droplet's conducting surface during the process of CEW. Under the one-dimensional geometry approximation, the ultimate electrical double layer (UEDL) due to the combined action of the FEDL and the addition of aluminum flakes undergoes a synthetic voltage drop in the following form:

$$V_{\mathrm{UEDL}} = -q_0/C_0 - Ex + V_{\mathrm{Al}} \times (x > 0) \tag{S5}$$

Where $x$ denotes the in-situ x-coordinate on the LM's surface to its mass center, $E$ the background DC electric field strength, $V_{\mathrm{Al}}$ the additional double-layer voltage drop existing preferentially on the right half side of the LM droplet caused by Al-mediated galvanic reaction. According to Lippmann's equation, the voltage-dependent surface tension coefficient at the sharp material interface between the LMD and working fluid is given by:

$$\gamma = \gamma_0 - \frac{1}{2}C\left(V_{\mathrm{UEDL}}\right)^2 = \gamma_0 - \frac{1}{2}C\left(-q_0/C_0 - Ex + V_{\mathrm{Al}} \times (x > 0)\right)^2 \tag{S6}$$

Where $\gamma_0$ denotes the maximum surface tension of reference in the absence of the electrical signal. $C$ denotes the capacitance per unit area of the FEDL, and $V_{\mathrm{UEDL}}$ the ultimate potential difference across the EDL. The result shows the surface tension is smaller in the region of a larger potential drop. Referring to Young's equation: $\Delta p = 2\gamma/R$, the static normal pressure drop $\Delta p$ across the droplet's interface and the tangential electrocapillary stress are respectively given by:

$$\begin{aligned} \frac{\partial \gamma}{\partial x} &= -CV_{\mathrm{FEDL}} \cdot \frac{\partial V_{\mathrm{FEDL}}}{\partial \mathrm{x}} \\ &= -C\left(-q_0/C_0 - Ex + V_{\mathrm{AL}} \times (x > 0)\right) \cdot \left(-E + \frac{V_{\mathrm{Al}}}{\delta} \times (0 < x < \delta)\right) \end{aligned} \tag{S7}$$

Here, it is assumed that there is a transition region with a characteristic horizontal length scale of $\delta$ to make the effect of aluminum sheet from null to stable. Besides, $\delta$ is sufficiently small in front of the droplet size. Ignoring the dipole shear stress component, Eq. S7 can be expressed as.

$$\frac{\partial\gamma}{\partial x} = -C_0\left[\frac{q_0}{C_0}E - \frac{q_0}{C_0}\frac{V_{\mathrm{Al}}}{\delta}\times\left(0<x<\delta\right) - EV_{\mathrm{Al}}\times\left(x>0\right) + \frac{{V_{\mathrm{Al}}}^2}{\delta}\times\left(0<x<\delta\right)\right] \tag{S8}$$

The global mean electrocapillarity stress is obtained by ignoring the localized force components that merely take effect in a small range as shown in Eq. S9.

$$\left\langle\frac{\partial\gamma}{\partial x}\right\rangle = -C_0\left[\frac{q_0}{C_0}E - EV_{\mathrm{Al}}\times\left(x>0\right)\right] = -q_0E + \frac{C_0EV_{\mathrm{Al}}}{2} \tag{S9}$$

The scale expression of the electro-capillary pump rate is obtained by the interfacial force equilibrium between the viscous stress and electrocapillary stress:

$$u = -\frac{q_0ER}{\eta} + \frac{C_0EV_{\mathrm{Al}}R}{2\eta} \tag{S10}$$

An interesting comparison between the first and second term on the right-hand side of Eq. S10 suggests that the role of aluminum sheet is in effect to enhance the negative surface charge density on the LMD's right half portion by the following amount:

$$q_{\mathrm{Al}} = -C_0V_{\mathrm{Al}} \tag{S11}$$

Then the Al-mediated electrocapillary pump flow velocity can be rewritten in the form below:

$$u = -\frac{ER}{\eta}\left(q_0 + \frac{q_{\mathrm{Al}}}{2}\right) \tag{S12}$$

As $q_0$ is generally negative, the positive voltage drop $V_{\mathrm{Al}}$ of the EDL owing to the negatively-charged aluminum with a surface-averaged charge density $q_{\mathrm{AL}}/2$ induces an additional pump flow component in the same direction as the original pump fluid motion driven by $q_0$. Therefore, the presence of aluminum flakes will accelerate the electrocapillary flow under the externally-imposed DC electric field. According to the Third Law of Newton's kinematics, the LMD moves in the opposite direction of the electric field line with a quicker translation speed as well.

## SI Appendix 3. Comparison of flow rate induced by the CEW of EGaIn and Al-EGaIn droplet.

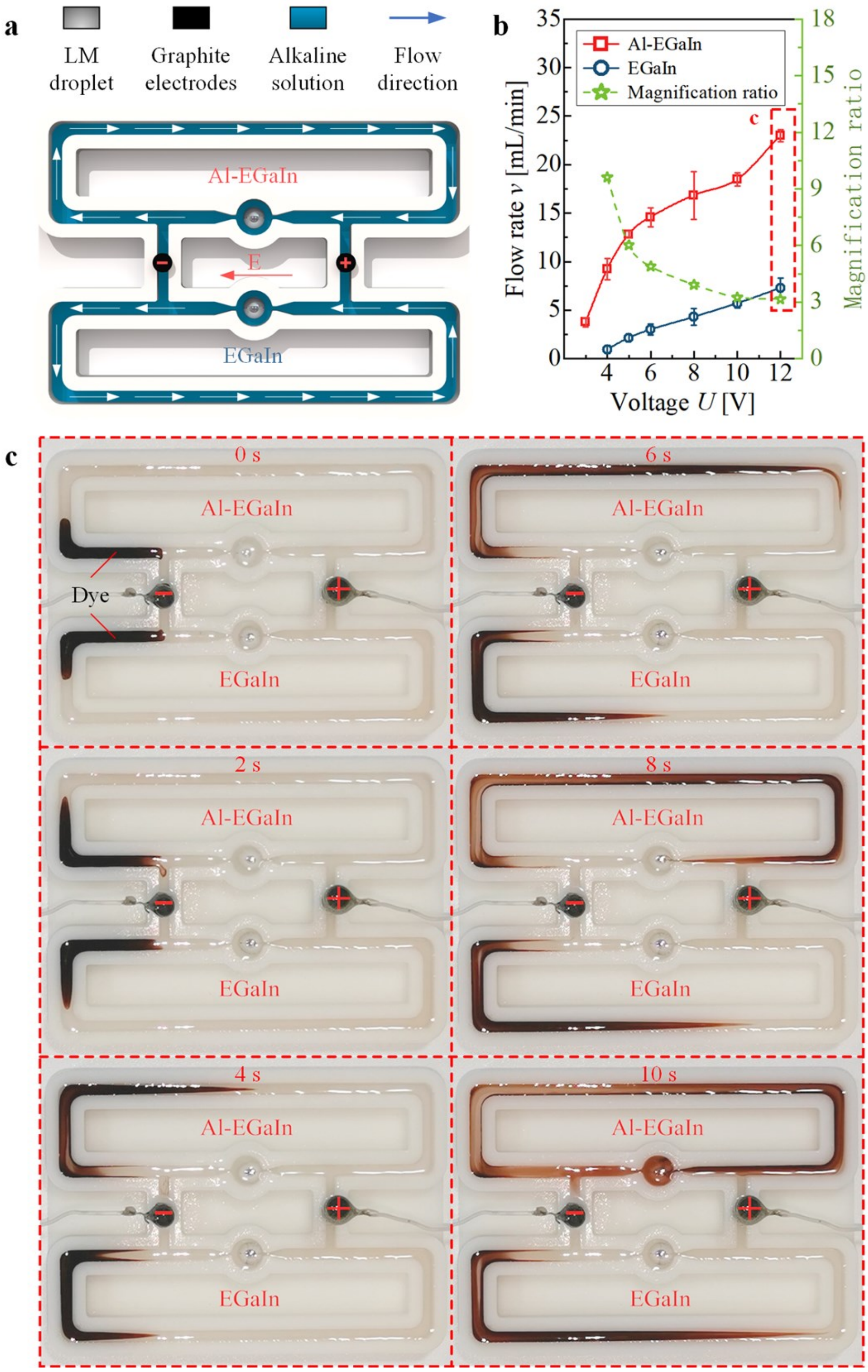


**Fig. S3.** Experiment to testify the influence of the electrical polarization of aluminium flakes on the CEW of the EGaIn droplet. a) Schematic of the test situation. b) Flowing rate vs. DC voltage (3

V~12 V) of the CEW induced on EGaIn/Al-EGaIn droplet's surface. Magnification ratio: Under the same conditions, the magnification times of CEW flow velocity induced by an Al-EGaIn droplet compared to that caused by a pure EGaIn droplet. c) Sequential snapshots of a record of flowing rate at 12 V. Two droplets of dye is used to demonstrate the pumping effect.

The EGaIn/Al-EGaIn droplets with the same volume of 100 μL were placed into the droplet chamber. The channel was filled with NaOH of 1 mol $L^{-1}$ and separated by a pair of graphite electrodes as shown in Fig. S3 a. Before the DC signal was applied, in the chamber of the Al-EGaIn droplet, the aluminum moving randomly on the droplet's surface with $H_2$ bubbles generating while no difference happened in the other chamber. When the external electric field was applied, the EGaIn/Al-EGaIn droplets began to move toward the anode and the solution flowed in the opposite direction. By increasing the magnitude of the DC voltage from 3 V to 12 V, the flow rates in the channel were also increased while the flow magnification due to the addition of aluminum decreases from 19 times (4 V) towards 3 times (12 V) as shown in Fig. S3 b and c, the final results suggest the introduction of aluminum enhances the CEW of the LMD, especially at the condition of low electric field intensity.

## SI Appendix 4. Force analysis of the power wheel

Seven different force components are acting on the rigid wheel as shown in Fig. 2 d: The forces applied to the wheel include the viscous resistance $F_{\text{inner}}$ from surface tension gradient induced flow, the viscous resistance $F_{\text{outer}}$ from the outer static aqueous solution in the water tank, the bearing friction torque $M$, the pressure of the LMD $F_{\text{n}}$ and rotation axis $F_{\text{N}}$, the gravity force $G$ and the buoyancy $F_{\text{buoyancy}}$. Among them, the viscous resistance $F_{\text{inner}}$ (marked with red) from surface tension induced flow as shown in Fig. 2 b and c is the impetus to turn the wheel. The viscous resistance $F_{\text{outer}}$ from the outer static aqueous solution and the bearing friction torque $M$ (marked with blue) are the obstruction to the rotating motion. When the power wheel operates in the steady-state with a constant rotation angular velocity, the effect of these 3 forces is balanced from physical constraint as follows:

$$F_{\text{inner}} R_{\text{inner}} = F_{\text{outer}} R_{\text{outer}} + M \tag{S13}$$

Where $R_{\text{inner/outer}}$ denotes the equivalent radius of the $F_{\text{inner/outer}}$. According to the Newton inner friction law: $F = \mu A \frac{du}{dy}$, as the flow velocity is related to its position, we simplify the calculation to only invoke the equivalent mean velocity. Besides this, although the viscous resistance $F_{\text{inner}}$ origin from 2 parts: The side and the bottom zone, since the effect and form of these double zones are quite similar, an equivalent analysis is performed during computation for mathematical simplicity. In this way, the $F_{\text{inner}}$ and $F_{\text{outer}}$ are respectively given by:

$$F_{\text{inner}} \approx \bar{F}_{\text{inner}} = \mu A_{\text{inner}} \frac{\bar{u}_{\text{surface}} - \omega R_{\text{inner}}}{y_{\text{inner}}} \tag{S14}$$

$$F_{\text{outer}} \approx \bar{F}_{\text{outer}} = \mu A_{\text{outer}} \frac{\omega R_{\text{outer}}}{y_{\text{outer}}} \tag{S15}$$

Where $A_{\text{inner/outer}}$ denotes the action area of $F_{\text{inner/outer}}$, $y_{\text{inner}}$ denotes the thickness of the thin liquid layer, $y_{\text{outer}}$ denotes the shortest distance between the outer wall of the power wheel and the inner surface of the tank's wall, $R_{\text{inner/outer}}$ denotes the equivalent moment arm of the $F_{\text{inner/outer}}$. It is assumed here that the flow velocity vanishes within the water tank far from the wheel.

According to Eq. S14 and S15, then Eq. S13 can be expressed as:

$$\mu A_{\text{inner}} \frac{\bar{u}_{\text{surface}} - \omega R_{\text{inner}}}{y_{\text{inner}}} R_{\text{inner}} = \mu A_{\text{outer}} \frac{\omega R_{\text{outer}}}{y_{\text{outer}}} R_{\text{outer}} + M \tag{S16}$$

Then the mathematic relationship between $\omega$ and $u_{\text{surface}}$ is given by:

$$\begin{aligned}\omega &= c_1 \bar{u}_{\text{surface}} + c_2 \approx c_1 u_{\text{surface}} + c_2 = c_1\left(-\frac{q_0 ER}{\mu} + \frac{C_0 E V_{\text{Al}} R}{2\mu}\right) + c_2 \\ &= \frac{c_1}{\mu}\left(-q_0 + \frac{C_0 V_{\text{Al}}}{2}\right) ER + c_2\end{aligned} \tag{S17a}$$

$$c_1 = \frac{y_{\text{outer}} A_{\text{inner}} R_{\text{inner}}}{y_{\text{outer}} A_{\text{inner}} R_{\text{inner}}^2 + y_{\text{inner}} A_{\text{outer}} R_{\text{outer}}^2} \quad c_2 = -\frac{y_{\text{inner}} y_{\text{outer}} M}{(y_{\text{outer}} A_{\text{inner}} R_{\text{inner}}^2 + y_{\text{inner}} A_{\text{outer}} R_{\text{outer}}^2)\mu} \tag{S17b}$$

Since the $y_{\text{inner/outer}}$, $R_{\text{inner/outer}}$, $A_{\text{inner/outer}}$, $M$, $\mu$ and $\eta$ are constants, $\omega \propto (-q_0 + C_0 V_{\text{Al}}/2)ER$. It is noteworthy that, since $q_0$ is negative and $V_{\text{Al}}$ is positive, the effects of fixed surface charge and the polarization of aluminum sheets coact synergistically in the same polarity, and therefore results in a counterclockwise rotating motion.

## SI Appendix 5. Real photo of the comparison channel

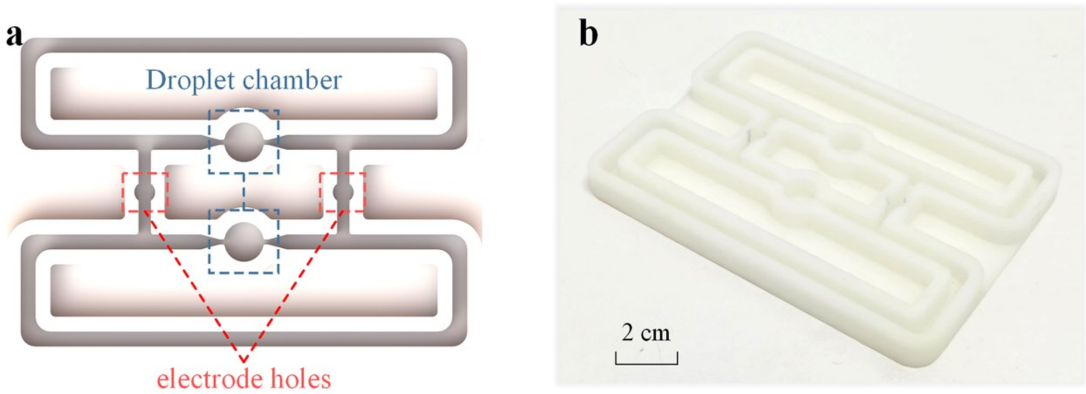


**Fig. S4.** Fabrication of the Test channel. a) Schematic of the test channel. b) Photo of the actual test channel.

The channel to investigate aluminum's effect for CEW is a closed-looped open-top double-cycle channel with a cross-section of 3 mm × 6 mm and a length of 220 mm separately as shown in Fig. S4 a. A cylindrical chamber with a diameter of 8 mm is designed in both channels for holding EGaIn/Al-EGaIn droplet and constraining its movement. A pair of electrode holes with a diameter of 4 mm is placed in the central line between these 2 channels to apply the same tunable electric field and cut off the fluidic flow between them. The whole structure is fabricated by 3D printing as shown in Fig. S4 b to ensure the consistency of actual machining dimensions.

## SI Appendix 6. Utilizing rotational motion to drive gear

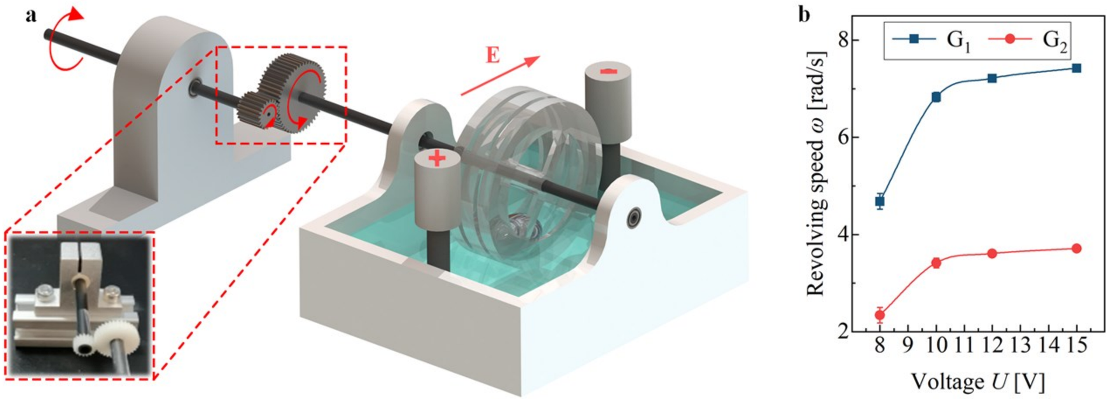


**Fig. S5.** Utilizing rotational output motion in gear drive. a) Schematic of the test channel ($Z_1$:$Z_2$=34:17). b) Revolving speed ($G_1$, $G_2$) $\omega$ vs. DC voltage (8 V, 10 V, 12 V, and 15 V).

The driven module can meet some conventional demands of low torque such as gear drive. As shown in Fig S5 a, this module becomes a power source to drive the capstan ($G_2$) in spur gear drive. Through meshing between the gear teeth, the final output rotation rate ($G_1$) can be adjusted by the ratio of teeth between gears. By adjusting the magnitude of the DC voltage within 8 V ~ 15 V (Fig.S5 b), the revolving speed of capstan varying from 2.34 rad/s ~ 3.71 rad/ which is half of the output rate.

## SI Appendix 7. Real photo of the circulating channel

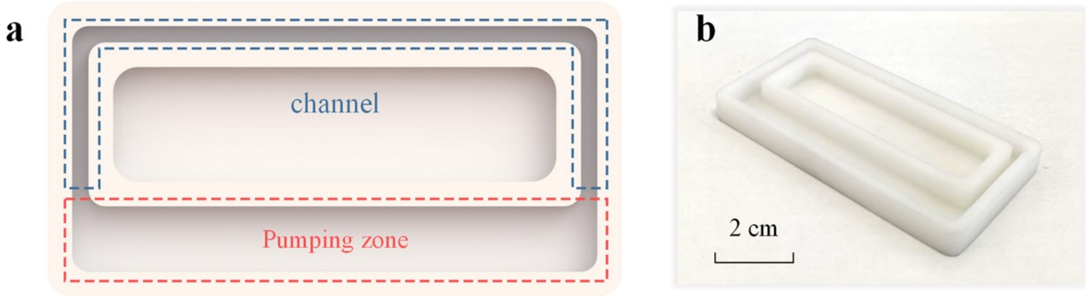


**Fig. S6.** a) Schematic of the circulating channel. b) Photo of the actual circulating channel.

The circulating channel for velocity measurement is a simple closed-loop open-top channel which can be divided into 2 parts as shown in Fig. S6 a: The pumping zone and the observation channel. The pumping zone is a cuboid region of 60 mm × 8 mm × 5 mm for holding the pumping wheel. The other part is the observation channel with a cross-section of 2 mm × 5 mm and a total length of 90 mm. It is also fabricated by 3D printing as shown in Fig. S6 b.

## SI Appendix 8. Redesign of the driven module to improve productivity

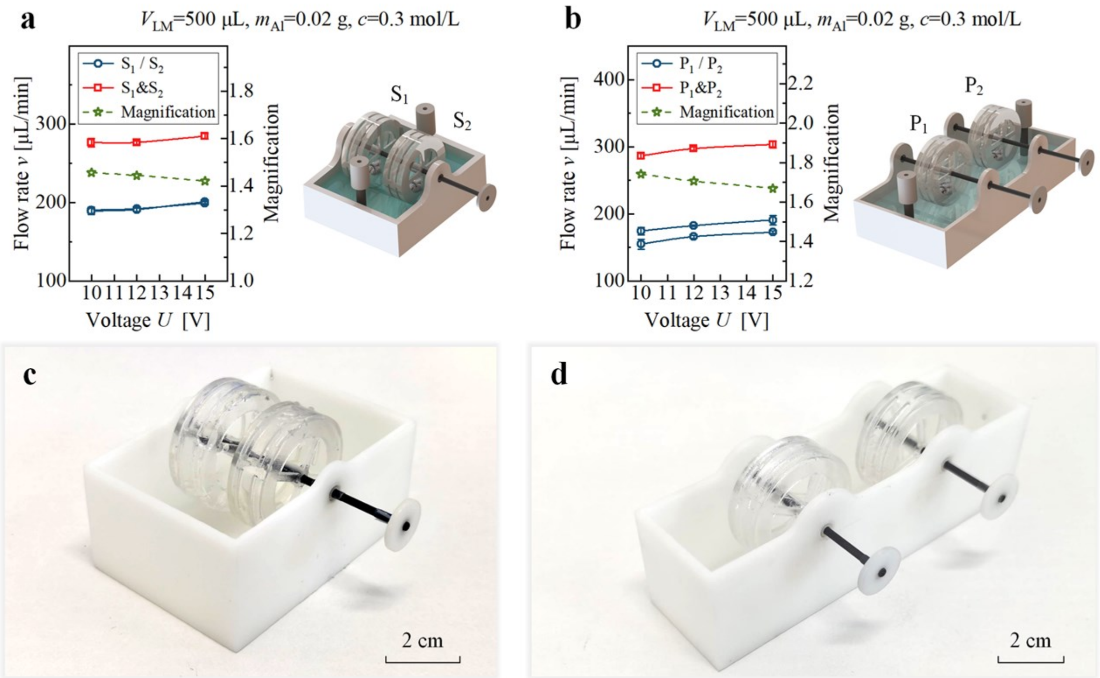


**Fig. S7.** Serial and parallel arrangement of the new driven module. a) Schematic of the circulating channel a Flow rate and efficiency improvement effect of the serial arrangement. b) Flow rate and efficiency improvement effect of the parallel arrangement. c) Photo of the actual serial arrangement structure. d) Photo of the actual parallel arrangement structure.

To improve the efficiency of this module, another driven wheel is added with 2 different connection types, serial (Fig. S7 a) and parallel (Fig. S7 b). Under a given applied voltage range of 10~15V, in comparison with utilizing only an individual driven wheel in the same module, the efficiency of serial arrangement with a pair of driven wheels can be improved by 1.45 times via an enhancement of the rotating axis's revolving speed. As to the parallel arrangement, the overall output speed is 1.65 times the average velocity generated when the two axes operate separately, mainly due to a larger contact area between the pump wheel and the liquid solution within the test channel. These results suggest the parallel arrangement mode of a pair of driven wheels can improve the pumping speed to a better degree than the serial arrangement configuration. Their mechanism forms are displayed in Fig. S7 c and d and the design parameters are shown in Table S2.

## SI Appendix 9. Biological driven module and cell culture channel

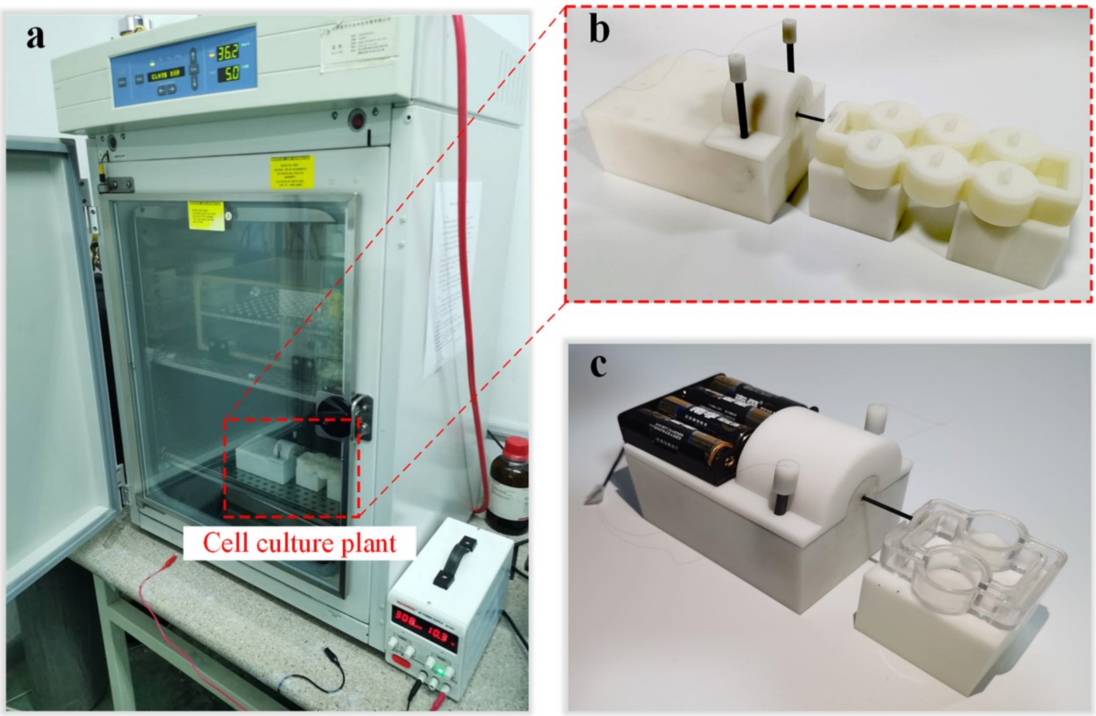


**Fig. S8.** a) Photo of the actual biological experiment.b) Photo of the actual cell culture plant. c) Dynamic cell culture platform with battery.

The ultimate bio experiment is conducted with a DC power supply due to a continuous power of 72 h and the cell culture plant is shown in Fig. S8 a. The dynamic cell culture can be powered by both power supply for a long time (Fig. S8 b) and batteries for a short period (Fig. S8 c).

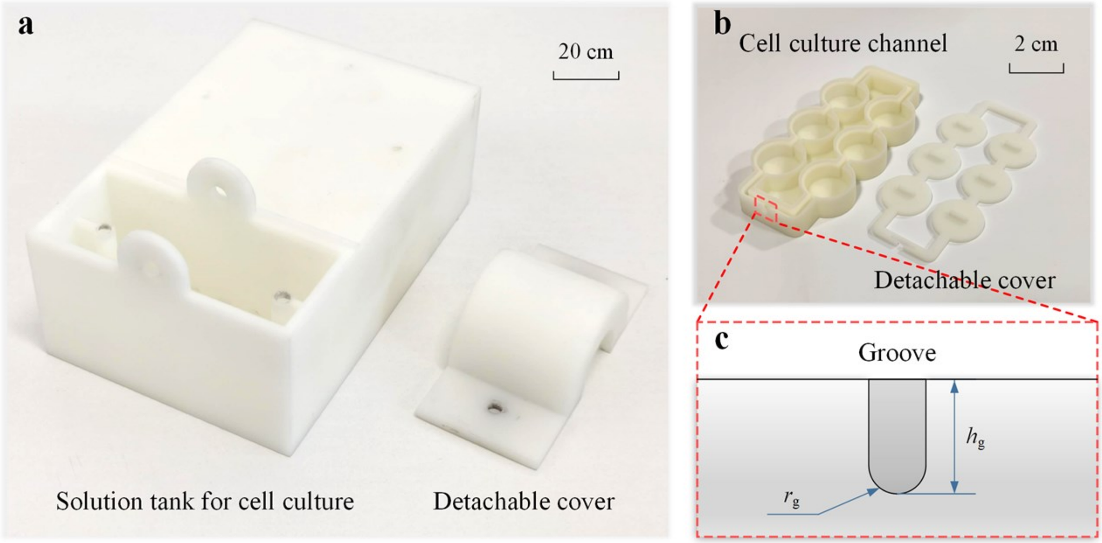


**Fig. S9.** a) Photo of the actual solution tank for cell culture. b) Photo of the actual cell culture channel. c) Detailed parameter of the groove.

The biological drive module is designed as a closed structure at the working state through a detachable cover plate for preventing solution volatilization in the cell incubator (37℃) as shown in Fig. S9 a. Another main difference from the original driven module is the volume of its tank. To hold enough NaOH solution for 8 h propulsion, the tank is designed as a cuboid shell of 120 mm × 80 mm × 45 mm (about 361 mL) with a wall thickness of 2 mm.

The cell culture channel is designed to provide a closed dynamic cultivation environment for the Hela cells as shown in Fig. S9 b. It includes two parts: A detachable cover and a channel that can accommodate up to 6 coverslips with Hela cells sample together. These six round shape cavities, each with a diameter of 12 mm, are connected one by one through a channel with a cross-section of 2 mm × 10 mm. A groove for the rotation axis to pass through is placed on one side of the cell culture channel and its detailed design para structural parameters are displayed in Fig. S9 c and Table S1.